A model-independent analysis of the variability of GRS 1915+105

Belloni, T.; Klein Wolt, M.; Méndez, R.M.; van der Klis, M.; van Paradijs, J.A.

[Link to publication](#)

A model-independent analysis of the variability of GRS 1915+105

T. Belloni[1,2], **M. Klein-Wolt**[1], **M. Méndez**[1,3], **M. van der Klis**[1], **and J. van Paradijs**[1,4]

[1] Astronomical Institute "Anton Pannekoek", University of Amsterdam and Center for High-Energy Astrophysics, Kruislaan 403, 1098 SJ Amsterdam, The Netherlands
[2] Osservatorio Astronomico di Brera, Via E. Bianchi 46, 23807 Merate (LC), Italy
[3] Facultad de Ciencias Astronómicas y Geofísicas, Universidad Nacional de La Plata, Paseo del Bosque S/N, 1900 La Plata, Argentina
[4] Physics Department, University of Alabama in Huntsville, Huntsville, AL 35899, USA

Abstract. We analyzed 163 observations of the microquasar GRS 1915+105 made with the Rossi X-ray Timing Explorer (RXTE) in the period 1996-1997. For each observation, we produced light curves and color-color diagrams. We classified the observations in 12 separate classes, based on their count rate and color characteristics. From the analysis of these classes, we reduced the variability of the source to transitions between three basic states: a hard state corresponding to the non-observability of the innermost parts of the accretion disk, and two softer states with a fully observable disk. These two soft states represent different temperatures of the accretion disk, related to different local values of the accretion rate. The transitions between these states can be extremely fast. The source moves between these three states following certain patterns and avoiding others, giving rise to a relatively large but limited number of variability classes. These results are the first step towards a linking of the properties of this exceptional source with standard black-hole systems and with accretion disk models.

Key words: black hole physics – stars: binaries: close – stars: individual: GRS 1915+105 – X-rays: stars

1. Introduction

GRS 1915+105 was discovered in 1992 with WATCH (Castro-Tirado et al. 1992) as a transient source with considerable variability (Castro-Tirado et al. 1994). It was the first Galactic object to show superluminal expansion in radio observations (Mirabel & Rodríguez 1994). The standard interpretation of this phenomenon in terms of relativistic jets (Rees 1966) placed the source at a distance D = 12.5 kpc, with a jet axis at an angle $i=70°$ to the line of sight (Mirabel & Rodríguez 1994; Rodríguez & Mirabel 1999; but see Fender et al. 1999). A counterpart has been found in the infrared (Mirabel et al. 1994), but the high Galactic extinction prevents the detection of an optical counterpart. Before the launch of the Rossi X-ray Timing Explorer (RXTE), not many observations of this source existed in X rays: the WATCH and SIGMA instruments on board GRANAT and BATSE/GRO showed once again that it was very variable in the X-ray band (Sazonov et al. 1994; Paciesas et al. 1996).

Since the launch of RXTE, the source has been monitored continuously with the All-Sky Monitor (ASM) instrument, which showed that the 2-10 keV X-ray flux of the source is extremely variable, unlike any other known X-ray source (see Remillard & Morgan 1998). GRS 1915+105 was observed extensively with the Proportional Counter Array (PCA) on board RXTE: from these data, the variability of the source appears even more extreme (Greiner et al. 1996). Quasi-periodic oscillations with frequencies ranging from 0.001 to 67 Hz have been observed (Morgan et al. 1997; Chen et al. 1997). A subset of observations, showing a remarkably regular behavior, has been presented by Taam et al. (1997) and Vilhu & Nevalainen (1998), with different interpretations. Other observations did not show spectacular variability (see Trudolyubov et al. 1999). The source is suspected to host a black hole because of its similarity with the other Galactic superluminal source GRO J1655-40 (Zhang et al. 1994), for which a dynamical estimate of the mass is available (Bailyn et al. 1995) and because of its very high X-ray luminosity.

Belloni et al. (1997a,b) showed, from the analysis of the energy spectra of selected observations, that the large variability of the X-ray flux of GRS 1915+105 can be interpreted as the appearing/disappearing of a detectable inner region of the accretion disk, caused by the onset of thermal-viscous instabilities. From the comparison of the X-ray color-color diagrams of all observations available until then, they showed that all observations were consistent with this interpretation, with the exception of a few, whose character could not be accounted for. Additional spectral analysis has been presented by Markwardt et al. (1999) and Muno et al. (1999), who analyzed in detail the connection between QPOs and X-ray spectral distribution in GRS 1915+105.

Quasi-periodic variability in the radio and infrared bands has been discovered (Pooley 1995; Pooley & Fender 1997; Fender et al. 1997). Fender et al. (1997) suggested that these oscillations correspond to small ejections of material from the system. Indeed, these oscillations have been found to correlate with the disk-instability as observed in the X-ray band (Pooley & Fender 1997; Eikenberry et al. 1998; Mirabel et al. 1998; Fender & Pooley 1998). This strongly suggests that (some of) the matter from

Table 1. The observation IDs of the pointing analyzed in this work. The letters I,J,K stand for 10408-01, 20187-02, and 20402-01 respectively. The second column indicates how many observation intervals are included in this class. The # indicates the individual observation interval. When no # is specified, all intervals are included.

Class	N.	Observation IDs
α	23	J-01-00,J-01-01,J-02-00(#2,#3,#5),K-22-00,K-23-00, K-24-01,K-26-00(#3,#4),K-27-00,K-28-00, K-30-01(#2), K-30-02
β	25	I-10-00,I-21-00,I-21-01(#1),K-43-00(#2),K-43-02, K-44-00,K-45-00(#1,#2,#3,#5),K-45-03, K-46-00,K-52-01,K-52-02,K-53-00,K-59-00(#2);
γ	22	I-07-00(#2,#3),K-37-00,K-37-02,K-38-00, K-39-00,K-39-02,K-40-00,K-55-00,K-56-00, K-57-00
δ	33	I-13-00(#1),I-14-00,I-14-01,I-14-02,I-14-03, I-14-04,I-14-05,I-14-07,I-14-08,I-14-09,I-17-00, I-17-03,I-18-00(#1,#2),I-18-01,I-18-04,K-41-00, K-41-01,K-41-02(#1),K-41-03,K-42-00,K-53-02(#2), K-54-00
θ	17	I-15-00,I-15-01,I-15-02,I-15-03,I-15-04,I-15-05, I-16-00,I-16-01,I-16-02,I-16-03,I-16-04, I-21-01(#2),K-45-02
κ	4	K-33-00,K-35-00
λ	10	I-37-00(#1,#2), I-38-00(#3,#4,#5),K-36-00,K-36-01,K-37-01
μ	18	I-08-00,I-34-00,I-35-00,I-36-00, K-43-00(#1),K-43-01,K-45-01, K-53-01,K-53-02(#1),K-59-00(#3)
ν	18	I-37-00(#3),I-40-00,I-41-00, I-44-00,K-01-00(#3),K-02-02(#4)
ρ	19	K-03-00,K-27-02,K-30-00,K-31-00, K-31-01,K-31-02,K-32-00,K-32-01,K-34-00, K-34-01
ϕ	18	I-09-00,I-11-00,I-12-00,I-13-00(#2,#3), I-17-01,I-17-02,I-18-00(#3),I-19-00,I-19-01,I-19-02, I-20-00,I-20-01
χ_1	30	I-22-00,I-22-01,I-22-02,I-23-00,I-24-00,I-25-00, I-27-00,I-28-00,I-29-00,I-30-00,I-31-00
χ_2	47	K-04-00,K-05-00,K-07-00,K-08-00,K-08-01,K-09-00,K-10-00, K-11-00,K-12-00,K-13-00,K-14-00,K-15-00, K-16-00,K-17-00,K-18-00,K-19-00,K-20-00,K-21-01,
χ_3	15	K-49-00,K-49-01,K-50-00,k-50-01,K-51-00,K-52-00
χ_4	49	I-31-00,I-32-00,I-33-00,I-38-00(#2),I-42-00,I-43-00,I-45-00, J-02-00(#1,#4,#6),K-01-00(#1,#2), K-02-02(#1,#2,#3),K-24-00,K-25-00,K-26-00(#1,#2,#5), K-26-01,K-26-02,K-27-01,K-27-03,K-29-00, K-30-01(#1),K48-00

the inner disk is ejected in form of a jet throughout the instability phase.

GRS 1915+105 displays a bewildering variety of variability modes (see Greiner et al. 1996; Belloni et al. 1997a,b; Chen et al. 1997; Nayakshin et al. 1999; Muno et al. 1999). In this paper, we present a classification of the different types of variability observed in the X-ray emission of GRS 1915+105 and we demonstrate that all the variations can be accounted for in terms of switching between just three main spectral states. All the observations are found to follow this characterization, which is model-independent. The structure of the paper is the following. In Sect. 2, we present the extraction techniques and the tools used for the analysis. In Sect. 3, we proceed to the classification of the observations and present the evidence for the three basic states. In Sect. 4, we discuss these results in terms of physical models, in particular in connection with the disk-instability model presented in Belloni et al. (1997a,b). A forthcoming paper will include detailed spectral modeling for a precise (and model dependent) characterization of these states.

2. Data extraction and color-color diagrams

We analyzed all observations of GRS 1915+105 made between January 1996 and December 1997 marked PUBLIC in the RXTE TOO archive (at heasarc.gsfc.nasa.gov), plus observation sequences 20187-02-01-00, 20187-02-01-01 and 20187-02-02-00, for a total of 163 observations. A list of the observations

can be found, subdivided in classes (see below), in Table 1. Each observation consists of one or more continuous intervals of data (called observation intervals) separated by earth occultations. Each observation interval has a maximum duration of $\sim$1 hour per interval. Our database contains a total of 349 observation intervals. For each observation interval we produced light curves with 1 sec time resolution in three PHA channel intervals: A:0-13 (2–5 keV), B:14-35 (5–13 keV), C:36-255 (13–60 keV) (energy conversion corresponding to PCA Gain epoch 3). We subtract a constant background level of 10, 20 and 100 cts/s in the A, B and C bands respectively, as determined from the analysis of typical background spectra. Although this is only an approximation, the high source count rate minimizes the effect of background variations. From these light curves we produced a total light curve (R=A+B+C) and two X-ray colors: HR_1=B/A and HR_2=C/A.

The analysis described below is based on different combinations of these three parameters, R, HR_1 and HR_2. The choice of the definition for the two X-ray colors was made to ensure the linearity of the resulting color-color diagram (CD): any linear combination of two spectral models lies on the straight-line segment connecting their locations in the CD.

The energy spectra of GRS 1915+105 are usually fitted with a model consisting of the sum of a power-law and a multicolor disk-blackbody, modified by interstellar absorption (see e.g. Belloni et al. 1997b). This model has become standard for the fitting of spectra of black-hole candidates. Fig. 1
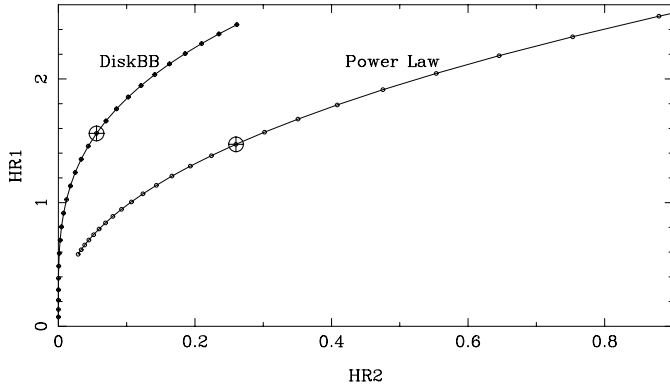
Fig. 1. Color-color diagram (CD) with the colors defined in the text. The two lines correspond to a power law with different photon indices Γ and to a disk-blackbody model with different inner disk temperatures kT_{in}. The adopted N_H value used is 6×10^{22}cm^{-2}. Temperatures increase by steps of 0.1 keV as the points move up, with the marked point corresponding to kT=2.0 keV. Power law indices increase by steps of 0.1 as the points move right, with the marked point corresponding to Γ=2.5.

shows a CD with the location of the two models for different values of their parameters (photon index Γ and temperature at the inner radius kT_{in}). The interstellar absorption has been fixed to 6×10^{22}cm^{-2}, as determined from spectral fitting (Belloni et al. 1997b, Markwardt et al. 1999). With our choice of colors, HR_2 is mostly sensitive to changes in the slope of the power law component and HR_1 to changes in the temperature of the disk component for the ranges shown in Fig. 1. The additional presence of an iron line or edge, although significant for the χ^2 fitting of energy spectra, does not modify the colors much compared to the overall range covered by the source. It is important to note that the color analysis is by itself independent of a specific model. Therefore, although we interpret the results in the framework of a power law plus disk model, all the observed color variations are model independent.

In addition to CDs, we also produced Hardness-Intensity Diagrams (HIDs), where HR_2 is plotted versus the total count rate. Although these diagrams contain absolute flux information and depend strongly on the long term variability of the source, in some case they are useful for characterizing the behavior during a single observation.

3. Data analysis

3.1. Selection of observations (classes)

Despite the extraordinarily complex variability displayed by GRS 1915+105, the examination of light curves and CDs shows that many features repeat in different observations. There are cases of observation intervals more than one year apart which are virtually indistinguishable from each other. We found that it was possible to classify our 349 observation intervals into only 12 classes, based on the appearance of light curves and CDs (see Table 1). This empirical classification is intended as a first step to reduce the complexity of the amount of available data,

as well as a way to present the overall picture of timing/spectral variability of GRS 1915+105 in a model-independent fashion. We outline the 12 classes below. One example for each class (light curve and CD) is shown in Fig. 2.

- class ϕ Two types of observations are relatively straightforward to separate from the others: those displaying no large amplitude variations (less than a factor of two) nor obvious structured variability (only random noise is seen in light curves binned at 1 second). However, examination of their light curves and CDs shows that these can be further subdivided into two separate classes: The first, class ϕ, is characterized by a count rate of $\sim$10 kcts/s or less and by a particular position in the CD, namely $HR_1 \sim 1$, $HR_2 \sim 0.05$ (see Fig. 2a,b).
- class χ The second, class χ, has a more varied count rate, ranging between 3400 and $\sim$30000 cts/s (for 5 PCU units) and it occupies a position in the CD which can vary but is always at $HR_2 > 0.1$ (see Fig. 2c,d). The cloud of points in the CD is usually diagonally elongated.
- class γ There are observations that are relatively quiet (class γ), apart from quasi-periodic oscillations with a typical time scale of $\sim$10 s and/or the presence of sharp 'dips' with a typical duration of a couple of seconds (see Fig. 2f). In the CD, the quasi-periodicity results in a diagonally elongated distribution of points. The points corresponding to the dips are separated from the main distribution, and are located on its left along the direction of the elongation (See Fig. 2e).
- class μ These are observations that, although showing large amplitude (more than a factor of two) variability, show a single 'branch' of points in the CD (class μ, Fig. 2g,h). This branch is elongated diagonally and it is curved to the right in its lower part. The light curves show rapid quasi-periodic oscillations (typical time scale between 10 seconds and 100 seconds), sometimes alternated with stabler periods of $\sim$100 seconds duration.
- class δ A number of observations show red-noise-like variability, which can exceed a factor of two in range. These observations form class δ. Notice that in a number of observations in this class, there are 'dips' in the light curve which, unlike the rest of the variability, are characterized by a significant softening in both colors (see Fig. 2i,j). These dips last typically 10-20 seconds and, while the out-of-dip count rate is always above 10000 cts/s, during the dip it decreases to 10000 cts/s or less.
- class θ A group of observations clearly distinguishable from the others is class θ (Fig. 2k,l): the light curve has a characteristic shape, with 'M' shaped intervals with a typical duration of a few hundred seconds, alternating with shorter (100-200 seconds) low count rate ($\leq$10000 cts/s) periods. In the CD, two separate distributions are seen: during the 'M' events HR_2 is above 0.1, while in the low-rate intervals it is considerably softer.
- class λ The observation presented in Belloni et al. (1997a) and a few similar ones constitute class λ (Fig. 2m,n): the light curve consists of the quasi-periodic alternation of low-
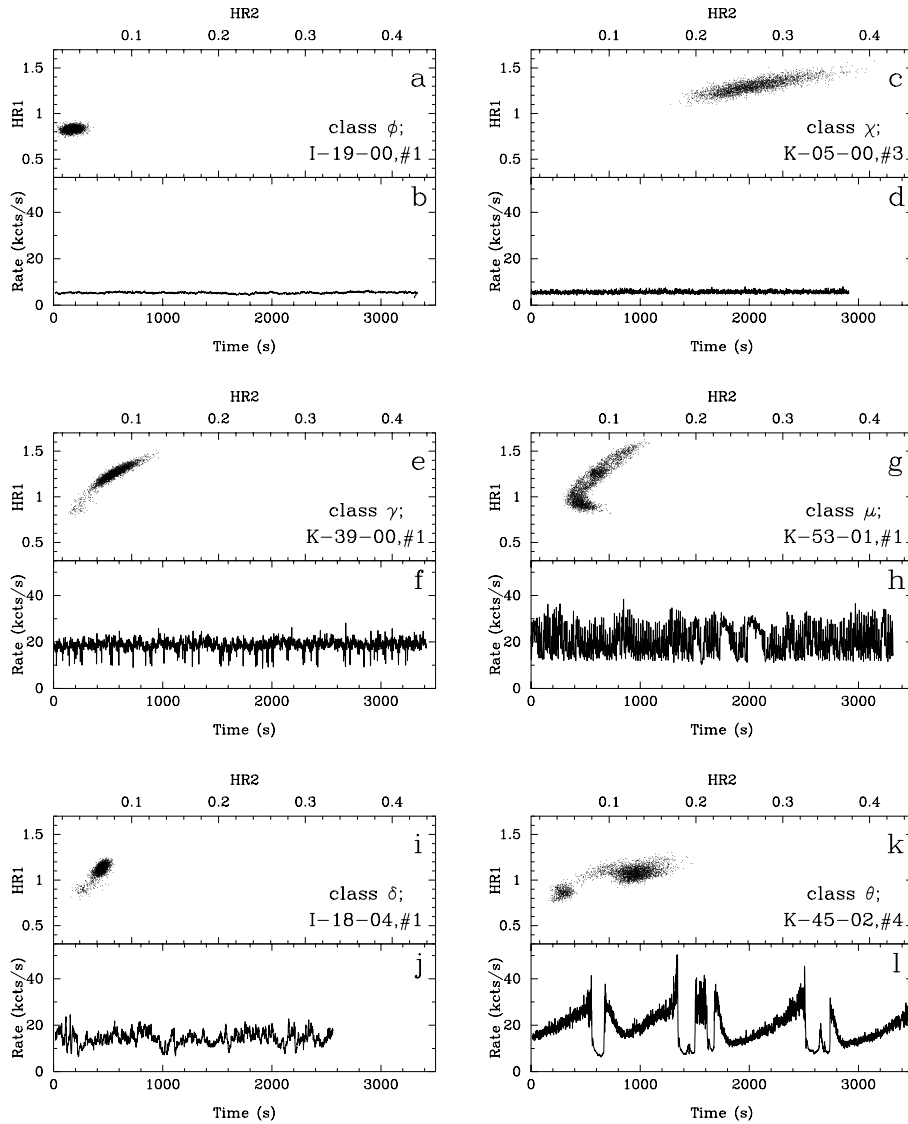
Fig. 2a – l. One example light curve and CD from each of the 12 classes described in the text. The light curves have a 1s bin size, and the CDs correspond to the same points. The class name and the observation number are indicated on each panel.

quiet, high-variable and oscillating parts described in Belloni et al. (1997a). In the CD, a C-shaped distribution is evident, with the lower-right branch slightly detached from the rest, and corresponding to the low count rate intervals (typically a few hundred seconds long).

- class κ Very similar to the previous class are observations in class λ. The timing structure, as shown by Belloni et al. (1997b), is the same, only with shorter typical time scales (Fig. 2o,p). In the CD, an additional cloud between the two branches is visible (see Belloni et al. 1997b).

- class ρ Taam et al. (1997) and Vilhu & Nevalainen (1998) presented extremely regular RXTE light curves of GRS 1915+105, consisting of quasi-periodic 'flares' recurring on a time scale of 1 to 2 minutes. There are differences in the observations presented by these authors, and for this reason we separate them in two classes. The first, class ρ (Fig. 2q,r), is extremely regular in the light curve, and in the CD it presents a loop-like behavior (described as ring-like

in Vilhu & Nevalainen 1998, where data with lower time resolution were considered).

- class ν There are two main differences between observations in this class and those of class ρ. The first is that they are considerably more irregular in the light curve, and at times they show a long quiet interval, where the source moves to the right part of the CD (see Fig. 2s,t). The second is that, at 1s time resolution, they show more structure in the profile of the 'flares', notably a secondary peak after the main one (see Fig. 17b).

- class α Light curves of observation intervals of class α show long ($\sim$1000 s) quiet periods, where the count rate is below 10000 cts/s, followed by a strong ($>$20000 cts/s) flare and a few 100s of seconds of oscillations(see Fig. 2u,v). The oscillations start at a time scale of a few dozen seconds and become progressively longer. This pattern repeats in a very regular way. In the CD, the quiet periods result in elongated clouds, the oscillations in small rings (not clearly visible
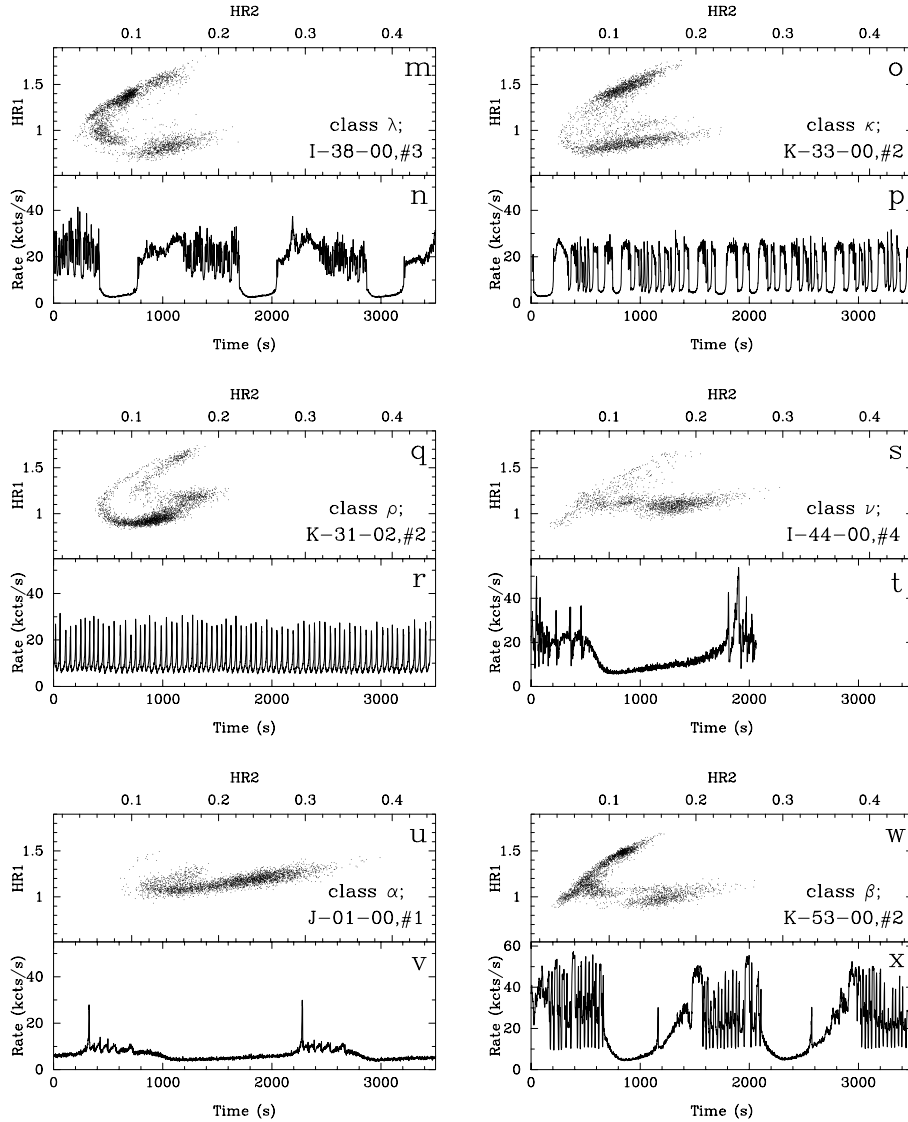
Fig. 2m – x.

in Fig. 2v) like those of classes ρ and ν, and the flare as a curved trail of soft (low HR$_2$) points (Fig. 2u).

- class β This class shows complex behavior in the light curves, some of which can be seen within other classes. What identifies class β however, is the presence in the CD of a characteristic straight elongated branch stretching diagonally.

The number of the classes presented above could be reduced, given the strong similarities between them, but our goal is not to have as few classes as possible, but to give as comprehensive a description of the source behavior as possible, in order to look for basic 'states' of the source. For this purpose, defining a relatively large number of classes means we are being conservative in order not to overlook important details in source behavior. All observation intervals in the sample considered for this work are covered by this classification, but it is quite possible that future observations would require yet other classes. Some of our observation intervals can be seen as boundary cases between two classes. Therefore, our classification is not intended to exhaustively list mutually exclusive modes of behavior for

GRS 1915+105 as: (i) transitions between some classes exist, (ii) a smaller number of classes would probably be sufficient to describe our observations, and (iii) more classes probably exist. The point of our work will instead be to demonstrate that this very complex behavior in fact follows a few very simple "universal laws". Summarizing, in Fig. 3 we show a histogram with the "occupation times" of the different classes in our sample. Noice that class χ is by far the most common.

3.2. Classes λ, κ and θ: the basic states

Two observations representing classes λ and κ, I-38-00 (Interval #3) and K-33-00 (Interval #2) respectively (notice the shortened naming convention, explained in the caption to Table 1), have already been presented by Belloni et al. (1997a,b). For a better understanding of what follows, we will briefly summarize their main result, restated using the terminology that we will use throughout the rest of this work. Let us start with examining class λ. The total light curve, the CD and the HID are shown in Fig. 4.
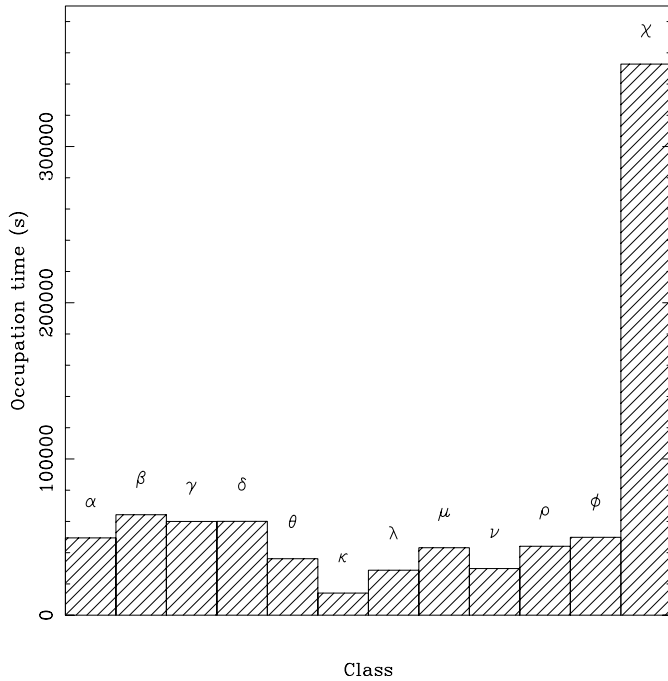
Fig. 3. Histogram of occupation time for each of the twelve classes.

Panels **a**, **b** and **c** in Fig. 4 are the HID, the light curve (restricted to the points used for CD/HID) and the CD respectively. The complete light curve of observation interval #3 is shown in panel **d**. Belloni et al. (1997a) identified in this observation (and then extended to all observations) three types of variability ("states"): a quiescent state at a relatively low count rate, an outburst state at high count rates, and a flare state in which the flux shows rapid alternations between the two. Hereafter, we will call the quiescent and outburst state C and state B respectively, and we will represent the corresponding points in all CDs, HIDs and light curves with squares and circles respectively. An example of these two states is clearly visible in Fig. 4. These are the two main states corresponding to the absence and presence of a detectable inner part of the accretion disk (Belloni et al. 1997a). The points corresponding to the two states cluster in two well separated regions of the CD and HID. In the CD, state B lies in the upper left part of the diagram, while state C is located more towards the lower right, at a higher HR_2 and lower HR_1. The flare state was interpreted by Belloni et al. (1997a) as oscillations between the other two, not as a separate state. An example of this is shown in Fig. 5, where the CD and HID for a "flaring" interval of the same observation are shown. It is evident that, although the high-flux points (state B, circles) are indeed located in roughly the same region of the CD as before, the low-flux points (state C, squares) are considerably softer than those from the long state C intervals in Fig. 4). From their analysis of observation K-33-00, Belloni et al. (1997b) showed that the position of the state C points in the CD depends on the length of the low-flux interval: the shorter the state C event is, the softer it is and the more it will be shifted to the left in the CD. Since the oscillations shown in Fig. 4 have a time scale considerably shorter than those in Fig. 2, a softening of the state C spectrum occurs. The identification of

these parts of the oscillations with state C is strengthened by the fact that during them 1-10 Hz QPOs are seen (see Markwardt et al. 1999; Muno et al. 1999).

On the basis of this analysis, Belloni et al. (1997a,b) tentatively concluded that the variability of GRS 1915+105 consists of oscillations between two separate states: state B corresponds to an accretion disk extending all the way down to the innermost stable orbit and therefore appears always with the same spectral colors, while state C corresponds to different portions of the inner disk being unobservable, and therefore can be found in different regions of the CD, but always at lower count rate and always separated from state B. However, Belloni et al. (1997b) also noticed that, although this characterization could be applied to most observations available at the time, one type of observation could not be reduced to these two states. This type observation is class θ in our classification of light curves (see Sect. 2). A typical observation of this class is shown in Fig. 6. The light curve consists of M-shaped intervals reminiscent of the long state C segments in Fig. 4. (although at a much higher flux level), alternated with low-rate stretches. In the middle of these low-flux stretches there are some 'flares'. Comparing the CD in Fig. 6 with that in Fig. 4, we can see that it is indeed plausible that the M-shaped intervals are consistent with being state C (at a slightly higher HR_1 and much higher count rate), and that the low-flux points cannot be identified with state B, being much softer. Since these soft points cannot be assigned to either of the two states, we define a new state (state A). In all the CDs, the points corresponding to this state will be marked with diamonds. During the 'flares' in the low-flux intervals, in the CD the source moves back almost to the state C points.

State A is characterized by consisting of low-flux, soft intervals, as opposed to state C, which is low-flux and hard. The presence of this additional state is very evident in an observation like that shown in Fig. 6, but in retrospect it could of course be present also in other observations. Going back to Fig. 4, we notice that at the end of a long state C period (see Fig. 4d) there is a short (<10s) dip. This dip corresponds to soft points in the CD (diamonds in Fig. 4c) which at the bottom of the dip reach the same position as those in Fig. 6. We find that in observations of class λ, this dip is *always* present as a transition between state C and state B, not only at the end of the long state C intervals, but also during the much more rapid flaring. By examining in detail the oscillations shown in Fig. 5, one can see that indeed a soft dip lies in between all C-B transitions, although the position in the CD in this case is much higher and in some cases it overlaps with that of state B (this overlap will be discussed extensively below). Also, the dip in the light curve corresponding to state A is not as deep as in the previous case.

Moving to observation K-33-00 (class κ), an examination of a short sample of the light curve shows that, although the time scales are shorter, the source behaves like in the λ case (see Fig. 7). This was already recognized by Belloni et al. (1997b), who based on these data their analysis of the disk instabilities for states B and C, but it also applies when state A is considered.
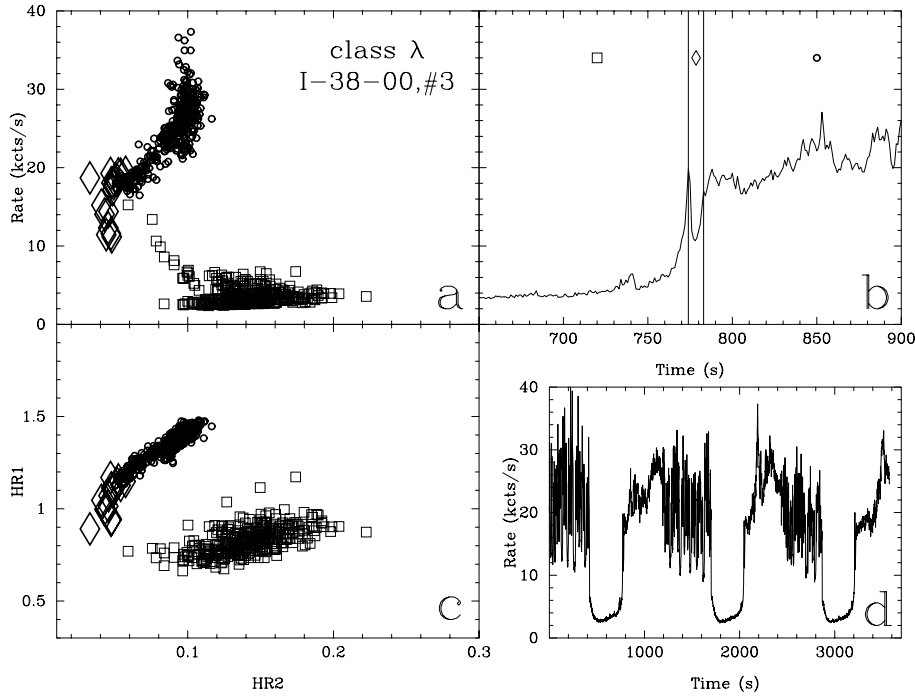
Fig. 4a – d. Sample observation from class λ. Panels **a,b,c** contain only part of the data, while panel **d** shows the whole dataset. **a** Color-intensity diagram; **b** light curve; **c** color-color diagram; **d** complete light curve. Diamonds, circles and squares correspond to states A, B, and C respectively. The vertical lines in panel b separate different states.
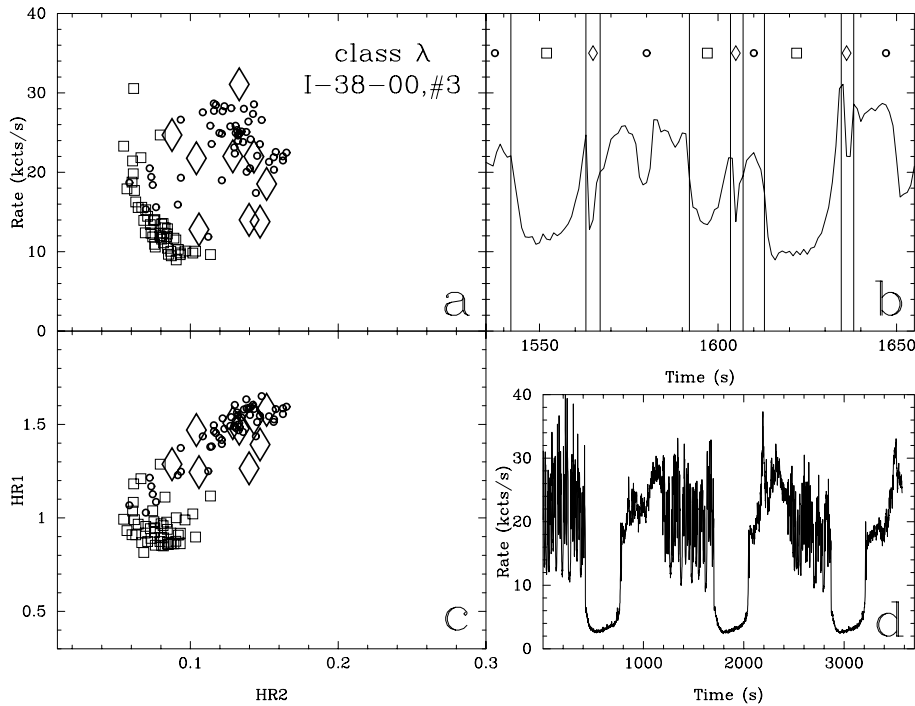

Fig. 5. Same as Fig. 4, but with a different subset of the observation selected for panels **a,b,c**.

3.3. The main color loop

It is useful to summarize the results from the first three classes before presenting more data. In the three observations we have discussed so far, we could identify three basic states:

- B : high rate, high HR_1;
- C : low rate, low HR_1, variable HR_2 depending on the length of the event;
- A : low rate, low HR_1 and HR_2

As far as the transitions between the three states go, in two cases (classes λ and κ), the source invariably follows the sequence: B -C -A -B and so on. In the third case (class θ), there are only oscillations between two states (C and A). No direct transition from state C to state B is observed. A schematical representation of this can be seen in Fig. 8. Notice that in some observations, state A is not completely separated from state B in the CD: this blending between the two classes is discussed exten-
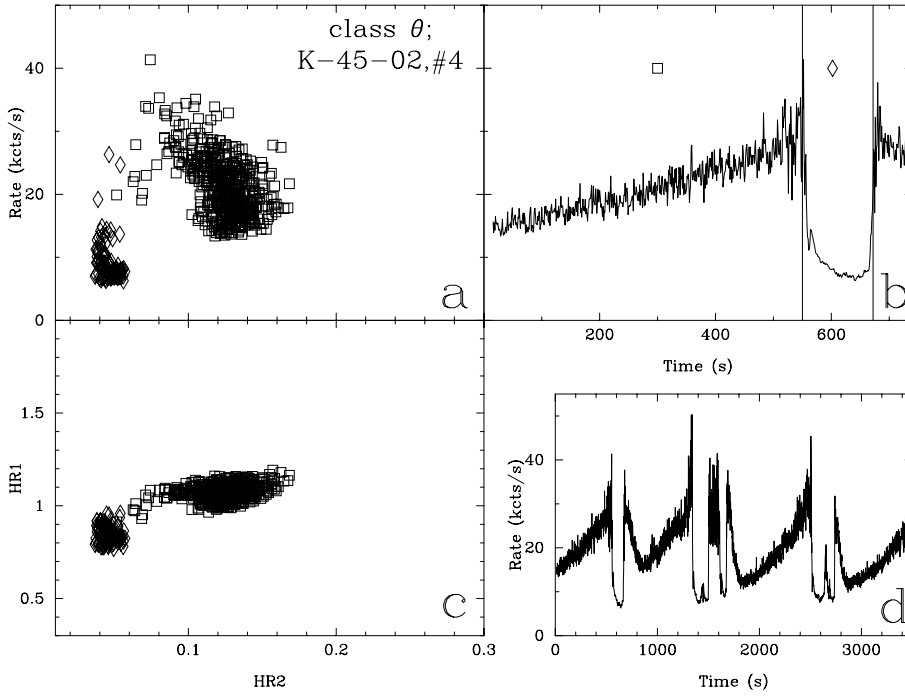
Fig. 6a – d. Sample observation from class θ. Panels **a,b,c** contain only part of the data, while panel **d** shows the whole dataset. **a** Color-intensity diagram; **b** light curve; **c** color-color diagram; **d** complete light curve. The symbols are the same as in Fig. 4

Fig. 7a – d. Sample observation from class κ. Panels **a,b,c** contain only part of the data, while panel **d** shows the whole dataset. **a** Color-intensity diagram; **b** light curve; **c** color-color diagram; **d** complete light curve. The symbols are the same as in Fig. 4
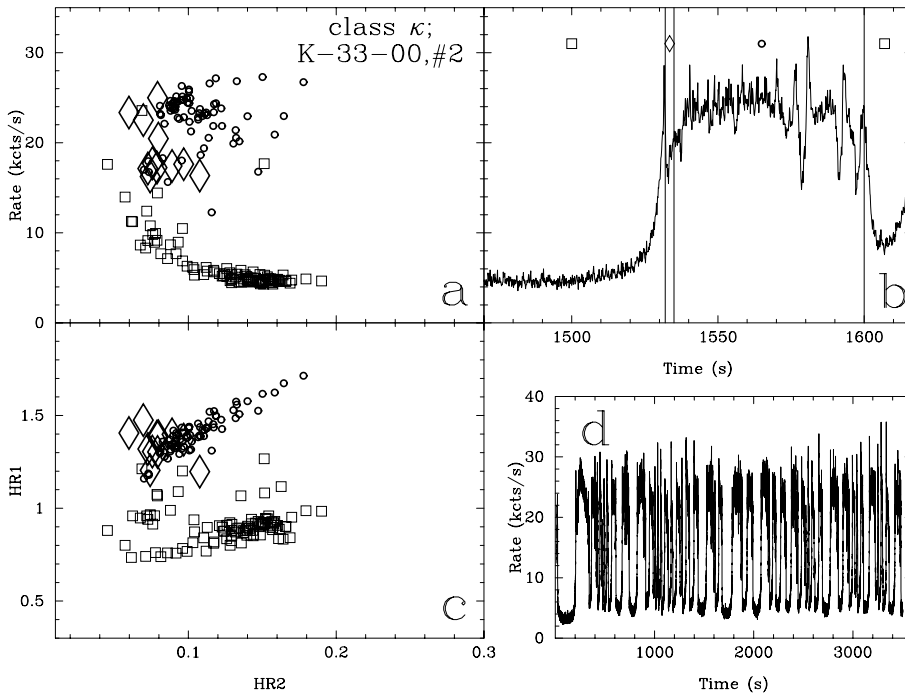
sively in the following sections. Before discussing this diagram however, we must go through the other classes.

3.4. Class χ: state C only

As described before, class χ is characterized by the absence of strong variability and $HR_2 > 0.1$. A large number of observation intervals belonging to this class correspond to observations taking place during three periods when no strong variability was observed on long (hours to months) time scales with the

RXTE/ASM. The three periods are identified in Fig. 9 by arrows. Although the two short such intervals are well defined in the ASM light curve (MJD 50280-50311 and MJD 50730-50750 respectively), the boundaries of the long one are not so clear. We define its start as the time after which *all* PCA observation intervals show no structure in the 1s light curves, and its end as the time after which structure in the time variability is observed again in the PCA. This leads to the following start-end times: MJD 50410-50550, corresponding to observations K-04-00 to K-21-01. Observation K-03-00, the last before this
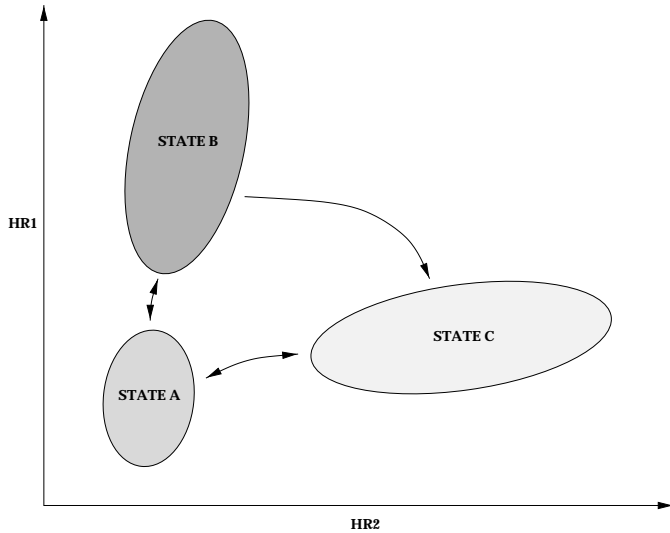
Fig. 8. Color-color diagram showing the basic A/B/C states and their observed transitions.
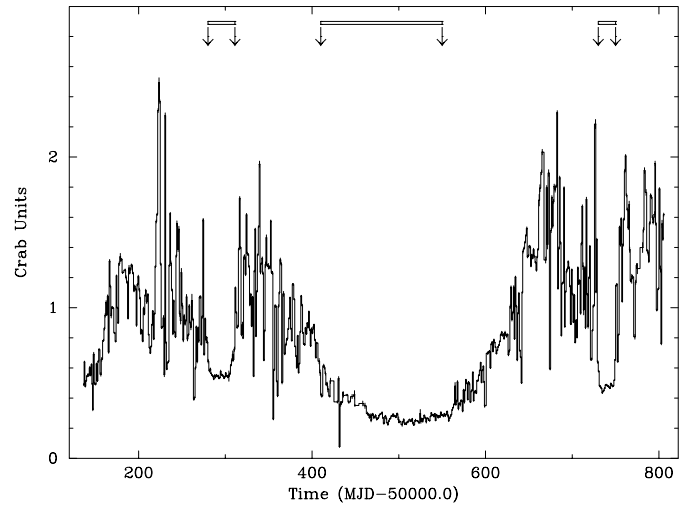

Fig. 9. RXTE/ASM light curve for the period analyzed in this paper. Bin size is 1 day. The bands in the upper part of the plot show the position of the quiet intervals examined in Sect. 3.4.

period, shows a clear quasi-periodic structure corresponding to class ρ, and observation K-22-00, the first after this interval, shows again a quasi-periodic structure, but classified as class α. Consistently, we applied the same method to re-define the time boundaries of the two shorter intervals, in order not to limit ourselves to the flat-bottom part of the light curves. We obtained the following time intervals: MJD 50275-50313 and MJD 50729-50750 respectively. We subdivided the observations of class χ into four sub-classes: χ_1, χ_2, χ_3 correspond to the three quiet intervals (in time sequence), while χ_4 comprises the remaining observation intervals, a number of which are located close to the long quiet interval. The assumption underlying this division is that the three long quiet intervals are indeed single intervals of no variability. Notice that our χ_1 and χ_3 intervals correspond to the "plateau" states in Fender et al. (1999). Fig. 10 illustrates a selection of four observations in this class. It can be seen that the position in the CD is similar to that associated to state C (see the previous section), and we therefore conclude that class χ is an example of state C only. The absence of flares and visible quasi-periodicities, as well as the presence of variability in the form of white noise at time scales of 1 second (see Markwardt et al. 1999 and Trudolyubov et al. 1999), further supports this identification as the same state as the low flux periods described in Sect. 3.2. However, it is clear that there is substantial spectral variability between different observations, as the clouds of points in the CD are found in quite different positions (Fig. 10). As mentioned in Sect. 3.2, for shorter events, the position of state C is also variable. In order to examine these variations, we computed the average values of the X-ray colors for each observation and plotted them into the same CD (Fig. 11). The lines corresponding to some spectral models are included in the plot. The points (filled symbols in Fig. 11) clearly distribute along three separate branches. Classes χ_2 and χ_4 follow a flatter trend than classes χ_1 and χ_3. From Fig. 11, one can see that large movements to the right in the CD are likely caused by harden-

ing of the power law component. However, a simple power law model with the "standard" value of $6 \times 10^{22} \text{cm}^{-2}$ for the interstellar absorption fits only the χ_1 and χ_3 points. On the basis of the CD, the other points (classes χ_2 and χ_4) can be fitted by a power law model with a lower absorption ($2 \times 10^{22} \text{cm}^{-2}$). An absorption of $2 \times 10^{22} \text{cm}^{-2}$ is compatible also with the χ_1 and χ_3 points only if an additional high-energy cutoff at ~ 5 keV is included (see lines in Fig. 11). Detailed spectral fits, which will be presented in a forthcoming paper, indeed indicate that both such a reduced absoption and a high-energy cutoff are present. Notice that $6 \times 10^{22} \text{cm}^{-2}$ is the standard value adopted for GRS 1915+105, while the lower value $2 \times 10^{22} \text{cm}^{-2}$ is still consistent with the galactic N_H as determined from radio measurements (Dickey & Lockman 1990). In this scenario, a large intrinsic absorption is present in the system and would be variable on a time scale longer than that of the long quiet intervals examined here.

3.5. Class ϕ: state A only

Class ϕ is the second of the two classes where no variability is observed. An example of light curve and CD is shown in Fig. 12 (upper panels). Compared to class χ, there is less white noise in the light curve (although in some cases red-noise variability is observed), and the points in the CD are much softer and more concentrated. The net count rate is <10 kcts/s. To determine whether this class corresponds to state A or state B , we need to compare the CD with that of an observation which shows both states. In Fig. 11 we show the average colors of all observations in class ϕ (see Table 1) together with the state B points from Fig. 4. By comparing Fig. 4c and Fig. 11, it is evident that observations in class ϕ have to be identified with state A . Note that the quietness of the light curve is also similar to the low-rate state A points from class θ (see Fig. 6). From Fig. 11, one can notice a continuity between state B and state A points, sug-
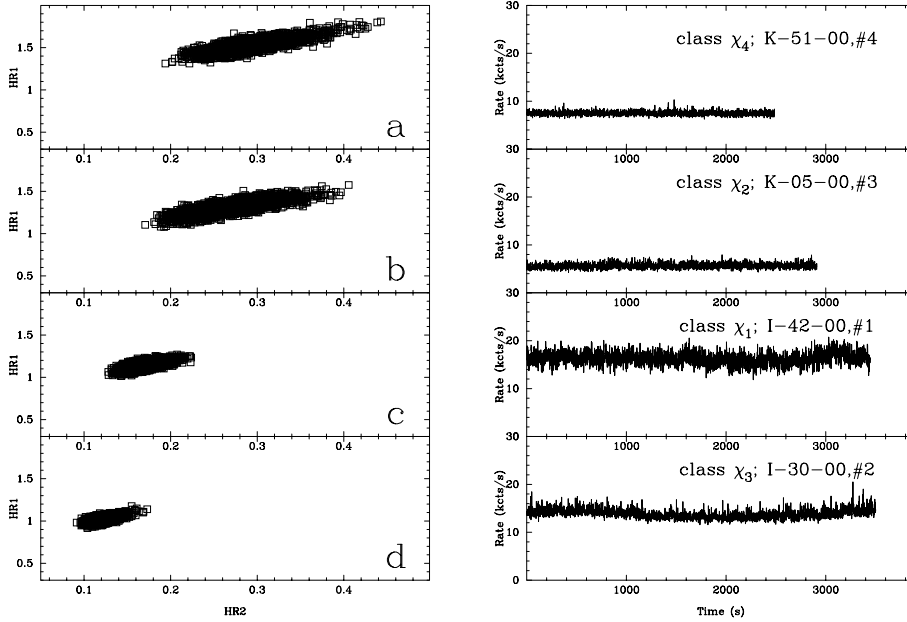
Fig. 10. Four examples of color-color diagrams (left) and light curves (right) for class χ.
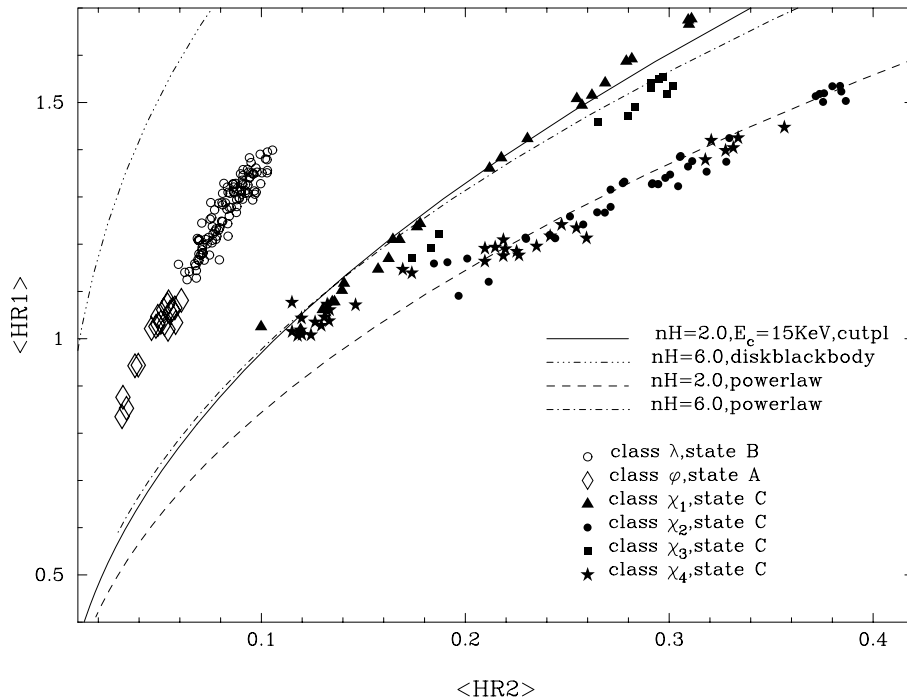

Fig. 11. Color-color diagram with the average values for observations in class χ, subdivided by sub-class (see text). Average points for observations in class ϕ are also shown as diamonds. Circles are the same circles in Fig. 3c. The lines show the expected positions of theoretical models (dbb=diskblackbody, pl= power law) for different values of N_H.

gesting that the two states might not be completely different but rather part of the same state. This will be discussed extensively below.

3.6. Class δ: B and A

An example of ligh curve, CD and HID for an observation in class δ is shown in Fig. 12 (lower panels). The light curve shows considerable 'flaring' variability. These variations are not accompanied by changes in X-ray colors, with the exception of a number of easily identifiable 'dips', which correspond to a spectral softening. From the CD, we can identify the dips as

occurrences of state A , while the rest of the time the source is in state B . It is noticeable that these state A events are the only ones when the source approaches or becomes weaker than 10 kct/sec.

3.7. Class μ

Observations from class μ show, like some parts of observations in class λ, large flaring variability and a characteristic shape in the CD: it is elongated diagonally and bends towards higher HR_2 values in its lower part (see Fig. 13). In panels b, c and d from this figure the part of the light curve used to produce the
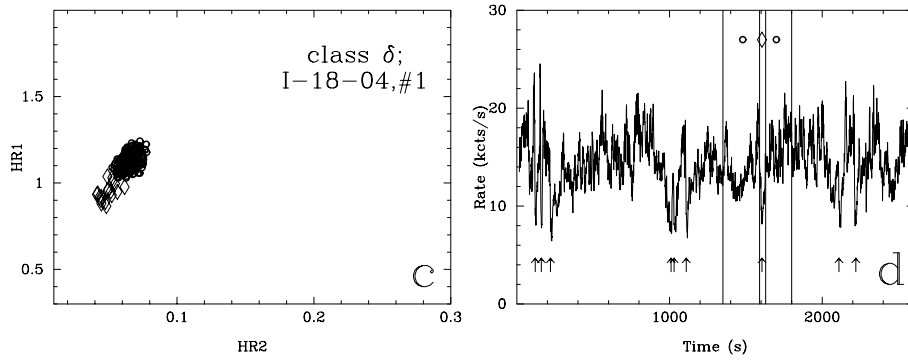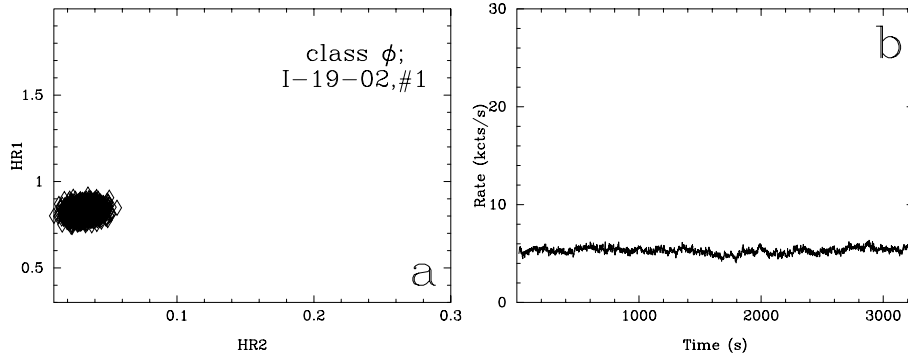
Fig. 12a – d. Panels **a,b**: CD and light curve of an example of class ϕ respectively. Panels **c,d**: CD and light curve of an example of class δ respectively. Points in panel c correspond only to the time intervals between the vertical lines, and are marked correspondingly. The arrows in panel d indicate the position of the state A transitions discussed in the text.
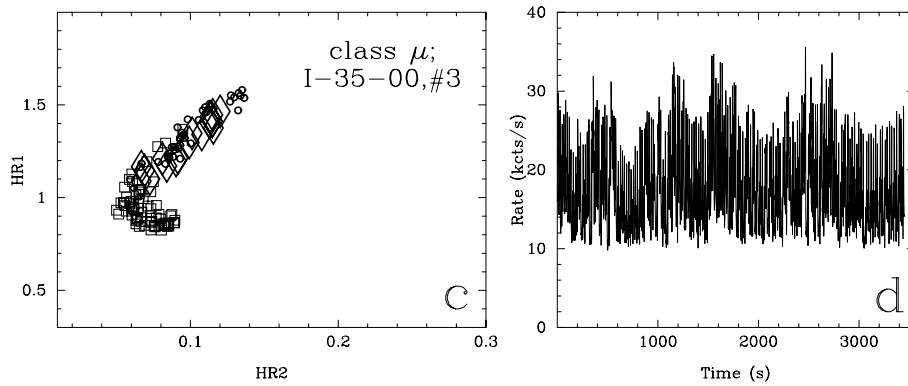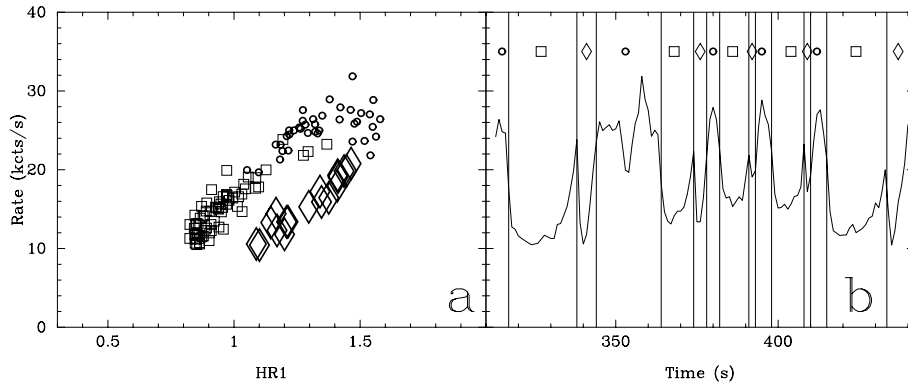

Fig. 13a – d. Sample observation from class μ. Panels **a,b,c** contain only part of the data, while panel **d** shows the whole dataset. **a** Color-intensity diagram; **b** light curve; **c** color-color diagram; **d** complete light curve. The symbols are the same as in Fig. 4

CD, the CD and the total light curve are shown respectively. When we compare this figure to Fig. 5, where the flaring state of observation I-38-00 (Orbit 3, class λ) is shown, the striking resemblance between the two is evident. We can therefore identify state C in both the light curve and the CD (Fig. 13).

Its relatively soft position in the CD compared to the position of state C in observation I-38-00 (Orbit 3) as shown in Fig. 4c, can again be explained by the short time scales observed (see Sect. 3.2). Although, from the light curve in Fig. 13b (and comparing this with the one shown in Fig. 5b) state A and B are
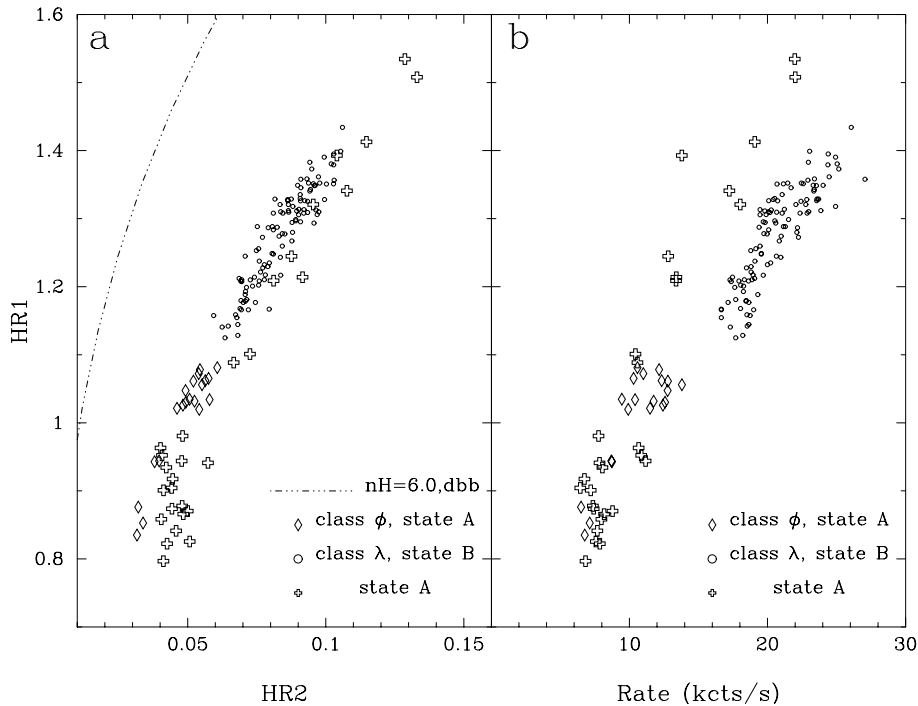
Fig. 14a and b. Panel **a**: color-color diagram. Circles and diamonds are the same as in Fig. 11. Crosses are dips to state A (see text). The dot-dash line corresponds to a disk-blackbody model with N_H fixed to 6×10^{22}cm^{-2}. Panel **b**: same points, but in a color-intensity diagram.

evident, they are not easily identified in the CD (Fig. 13c). The two states seem to be spectrally identical, as they take the same position in the CD. In order to check whether there is indeed a difference between state A and B, we produced a HID from the count rate and the HR1 values, again using only the part of the light curve shown in Fig. 13b. From this HID, shown in Fig. 13a, and the light curve in Fig. 13b, we see that in this class state A is also present, although its major difference with state B is count rate. State A and C both have count rates between 10 and 25 kcts/s, and only in state B the source becomes higher than 30 kcts/s.

Besides the rapid state alternations, stabler periods where the count rate remains at a high level around 40 ckts/s are observed in some light curves in class μ (see Fig. 2h). During these intervals hardly any spectral variation is seen, and the source takes a position in the CD with relatively soft HR2 (below $\sim$0.12) and hard HR1 (above $\sim$1.0) values. We therefore identify these intervals as periods where the source remains in state B for an extended period of time. They can be compared with the state B intervals in Fig. 4. Although at a higher count rate, the position in the CD is the same.

3.8. Variations within state A

As we have seen, in some cases examined so far the distinction between classes A and B in the CD becomes uncertain, complicating the simple picture sketched in Fig. 8. This is summarized in Fig. 14a, where we plot the CD from state B in observation I-38-00 (Orbit 3) and the average CD from class ϕ, as already shown in Fig. 11, together with the dips of all state A points shown in the previous sections. Indeed, most of state A points are clearly separated from those of state B, but some are not and

a couple of them are even harder than all state B points shown. However, if the same points are plotted in a HID (see Fig. 14b), those 'peculiar' state A points are immediately distinguishable from the state B ones. What can be seen in Fig. 14b is that the colors of both state A and state B points are correlated with the count rate, but follow different branches.

From Fig. 14, we can re-define state A in the following terms:

1. in the light curve, a sharp dip, with a typical transition time scale between out-of-dip and dip of a few seconds;
2. at low count rates (below 15 kcts/s), the position in the CD is relatively soft (HR$_1$ <1.1) and separated from state B;
3. at higher count rates, the position in the CD overlaps with that of state B, but follows a different branch in the HID, located at lower rates.

This branch will be examined in more detail below.

3.9. Class γ

In Fig. 15 we show observation K-39-00 (Orbit 1), representing class γ. All observations from this class have a count rate centered around $\sim$20kcts/s, and show evidence of quasi-periodic oscillations with period $\sim$60-100 s (see Fig. 15d), in some cases with an amplitude as high as a factor of two (see Greiner et al. 1996 and Morgan et al. 1997). Simultaneously, faster $\sim$10 s QPOs are observed (see Fig. 15b). A number of observations show also sharp dips as the ones observed in class δ. These dips always occur in correspondence to a minimum in the low-frequency oscillations.
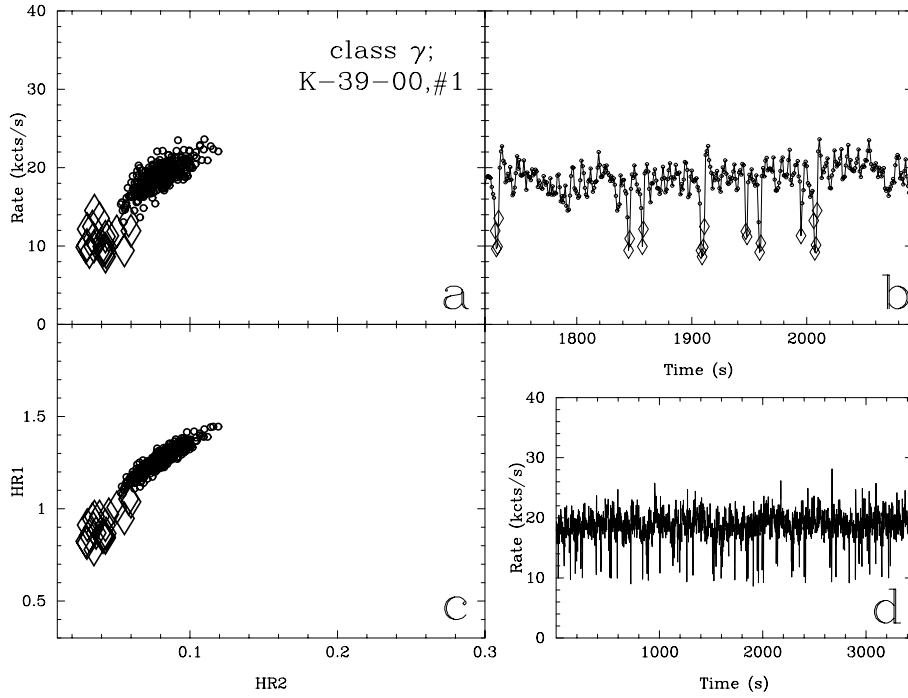
Fig. 15a – d. Sample observation from class γ. Panels **a,b,c** contain only part of the data, while panel **d** shows the whole dataset. **a** Color-intensity diagram; **b** light curve; **c** color-color diagram; **d** complete light curve. The symbols are the same as in Fig. 4

Fig. 16a – d. Sample observation from class ρ. Panels **a,b,c** contain only part of the data, while panel **d** shows the whole dataset. **a** Color-intensity diagram; **b** light curve; **c** color-color diagram; **d** complete light curve. The symbols are the same as in Fig. 4
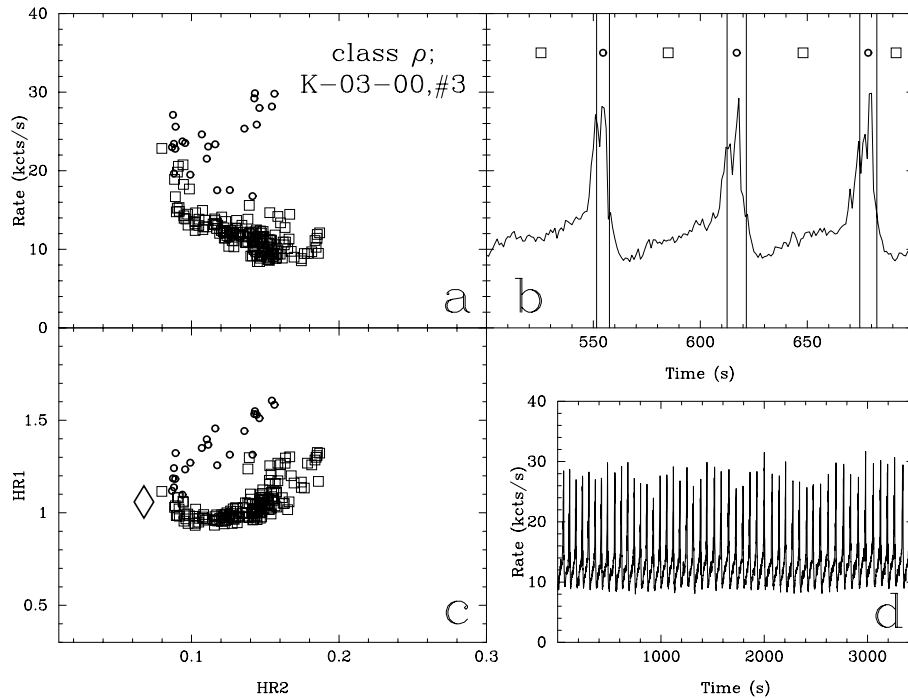
In the CD (Fig. 15c), by comparison with previous cases, it appears that the oscillations belong to state B and the dips to state A (compare Fig. 15c with Fig. 14a).

3.10. Class ρ and ν

Observations in class ρ have been presented by Vilhu & Nevalainen (1998), although limited to low time resolutions (16 seconds). The light curve consists of a very regular and characteristic pattern, which repeats on a time scale between one and two minutes (see Fig. 16). As noticed by Vilhu & Nevalainen (1998), these regular variations are reflected in a clockwise loop in the CD (Fig. 16). Notice that at a resolution of 1 second, the CD looks much less circular than in Vilhu & Nevalainen (1998), who used a resolution of 16 seconds, clearly not sufficient for the analysis of these observations. A comparison with the classes examined in the previous sections clearly indicates that the loop is constituted by oscillations between state B (high count rate) and state C (low count rate), without a clear evidence of a state A. However, when examining the light curves at a higher time
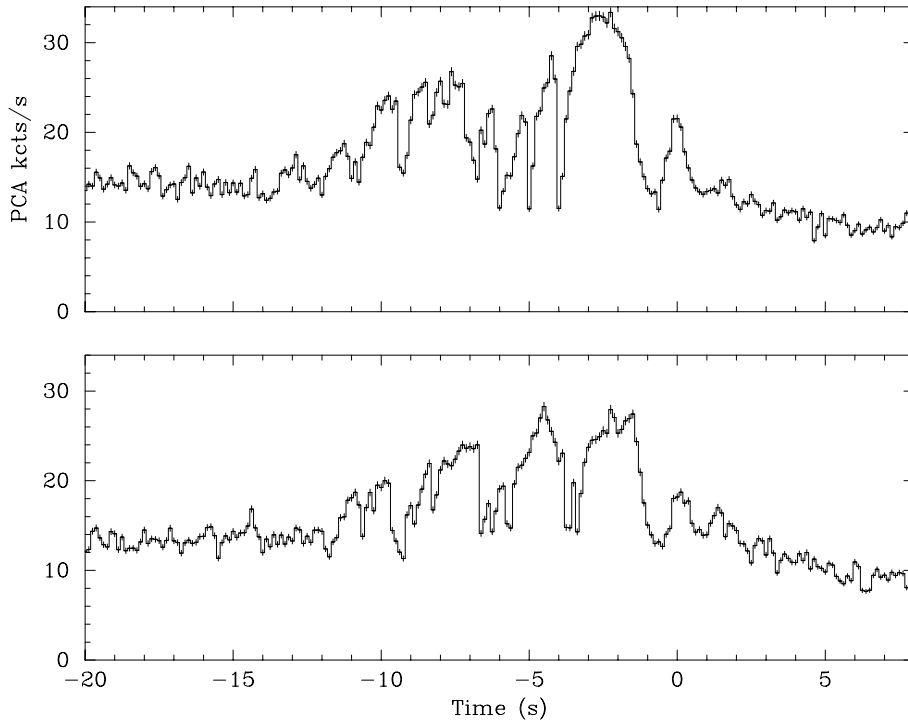
Fig. 17. Two examples of light curves at high (1/8 sec) time resolution light curves from observation K-03-00, shifted so that the small peaks at the end of the event match in time.

resolution, a complex type of variability is resolved (Fig. 17). The high count rate part of the cycle shows sharp dips, with count rate changes of a factor of 3 in less than one second. The overall structure of this variability does not repeat between different events, with the only exception of the small peak after the last dip. The two examples in Fig. 17 are shifted so that this peak corresponds to time 0. At such high time resolution it is difficult to follow a few points in the CD, since the count rate in the high-energy band becomes uncertain. From the observation in Fig. 16 and 16, binned at 1/8 s, we considered only the points in the 10 seconds preceding the last peak (in order to isolate the high count rate sections), and averaged the colors of the points with a total rate <12 kcts/s. The resulting average colors are indicated by the diamond in Fig. 16c: the point falls in the soft region of the CD plane, corresponding to the position of state A. All the states are therefore represented in the light curves of this class. Notice that for a few observations in this class, the high time resolution light curve is much smoother, but still the dip preceding the last peak is present.

An observation from class ν has been presented by Taam et al. (1997). In the light curve, class ν looks rather similar to the previous one (see Fig. 18). The main differences with class ρ are the possible presence of long quiet intervals between trains of oscillations (not shown in the example considered here, but see Fig. 2), the different characteristic shape in the 1s light curve, and the lower regularity of the oscillations. The very fast dips observed in class ρ can also be seen here, but are less deep. The long quiet interval, followed by a short high flux flare sometimes observed in observations included in this class (see Sect. 3.1) is very similar to that in class α and λ so it will not be discussed here. The difference in the regular light curve of class ν with respect to class ρ consists in the presence of a dip at the end

of the high-rate part of the cycle, which creates a secondary peak. This is reminiscent of the dip which gives origin to the small peak in class ρ, although in this class the dip and the peak are much longer, being both a few seconds long. By looking at the CD, one can see that the smooth clockwise movement from class ν is here interrupted during its ascending part by the dip, which is very soft. After the dip, the source moves to the hard part of the diagram. Following the structure of the previous sections, we can identify the long slow rise in the light curve with state C, followed by state A (the dip) and state B (the recovery from the dip, showing up as a secondary bump). Notice that in this class, the typical colors of both state B and state A are considerably harder than in most of the cases described in the previous sections.

3.11. Class α

The light curves from observations belonging to class α show a repetitive pattern of long (~ 1000 s) quiet intervals and periods were a strong (up to ~ 30 ktcs/s) flare is followed by a sequence of smaller oscillations (see Fig. 19d). The length of these oscillations increases with time and often their peak intensity decreases. The quiet intervals mentioned above can easily be identified with state C. They show the characteristic shape in the CD (Fig. 19c) and in the light curve(Fig. 19b), also seen in previous cases (see Fig. 4 and 6). The strong peak following each quiet interval looks practically identical to the quasi-periodic ones from class ρ (Fig. 16). Not only do they have the same shape in the light curve (compare Fig. 19b and 19e with Fig. 16b), they also show the same loop in the CD. This can be seen in Fig. 19f, were the CD belonging to the peak from Fig. 19e is shown. Therefore, during this peak the source moves
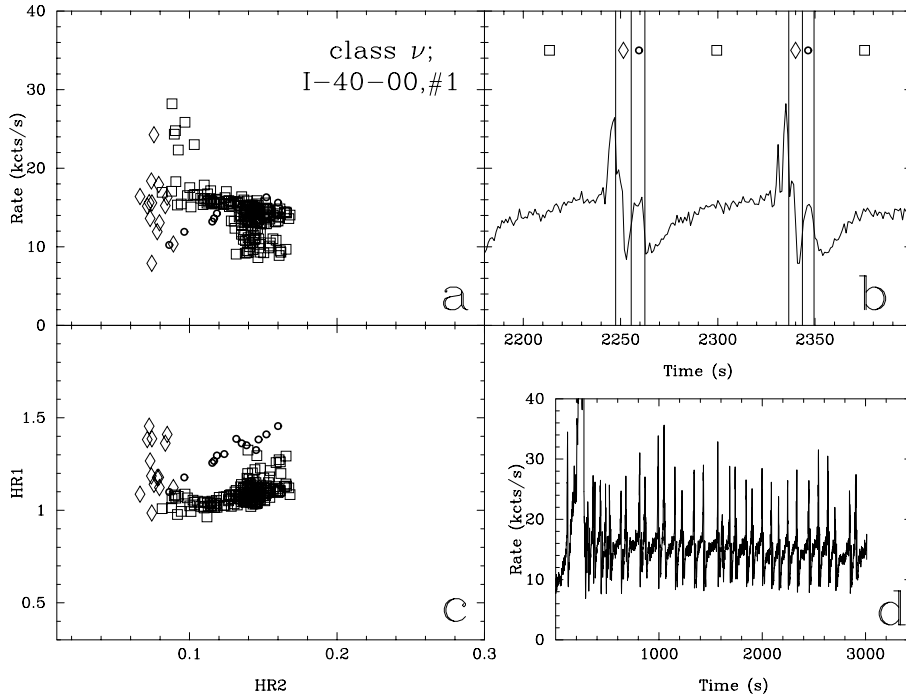
Fig. 18a – d. Sample observation from class ν. Panels **a,b,c** contain only part of the data, while panel **d** shows the whole dataset. **a** Color-intensity diagram; **b** light curve; **c** color-color diagram; **d** complete light curve. The symbols are the same as in Fig. 4
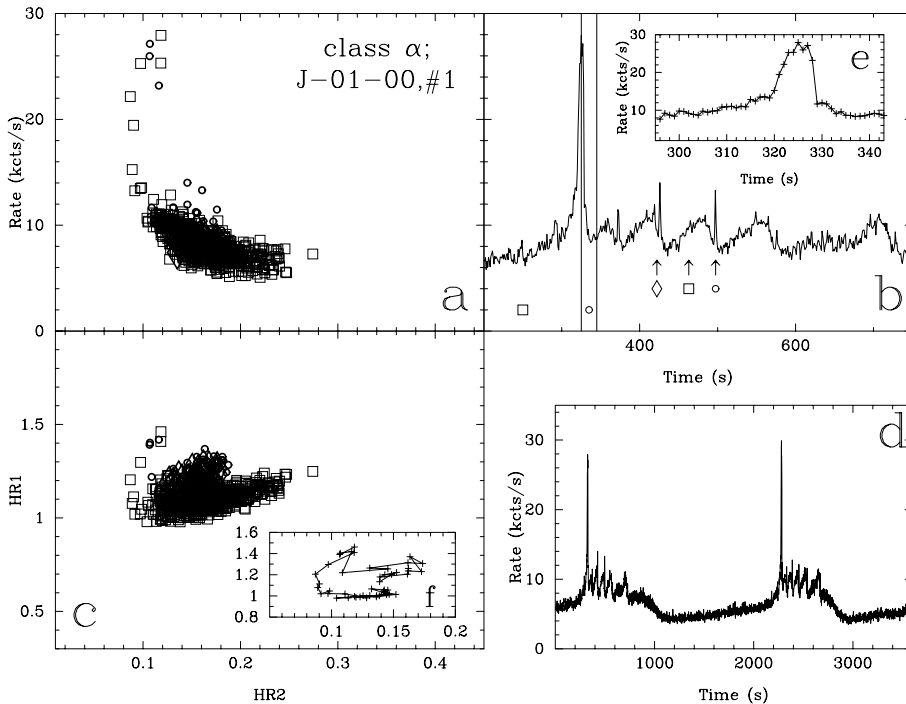
Fig. 19a – f. Sample observation from class α. Panels **a,b,c** contain only part of the data, while panel **d** shows the whole dataset. **a** Color-intensity diagram; **b** light curve; **c** color-color diagram; **d** complete light curve. The symbols are the same as in Fig. 4. Panel **e** shows an enlargement of the biggest peak, and panel **f** shows the corresponding CD.

through all the three states as explained in Sect. 3.10. In some observations, the initial strong peak shows a marked HR2-soft 'dip' similar to that observed in class ν (Fig. 18). All the smaller oscillations resemble the ones shown in Fig. 18 for class ν.

3.12. Class β

Observations grouped in class β show a large variety of complex behavior and for this reason are described as last, in order to

highlight the similarities with other classes. An example of this can be seen in Fig. 20d and Fig. 20b, were we show observation K-45-03 (Observation interval #1). Periods of large variability (between ~ 8 and ~ 40 kcts/s), similar to those seen in class λ (see Sect. 3.2), are alternated by quiet intervals. These quiet intervals are similar to those from observations in class θ, the main difference being the fact that here the dip phase after the strong peak is much less deep. The resulting CD (Fig. 20c) is characterized by a long elongated cloud stretching diagonally,

Fig. 20a – e. Sample observation from class α. Panels **a,b,c** contain only part of the data, while panel **d** shows the whole dataset. **a** Color-intensity diagram; **b** light curve; **c** color-color diagram; **d** complete light curve. The symbols are the same as in Fig. 4. Panel **e** shows an enlargement of an oscillating section of the light curve.
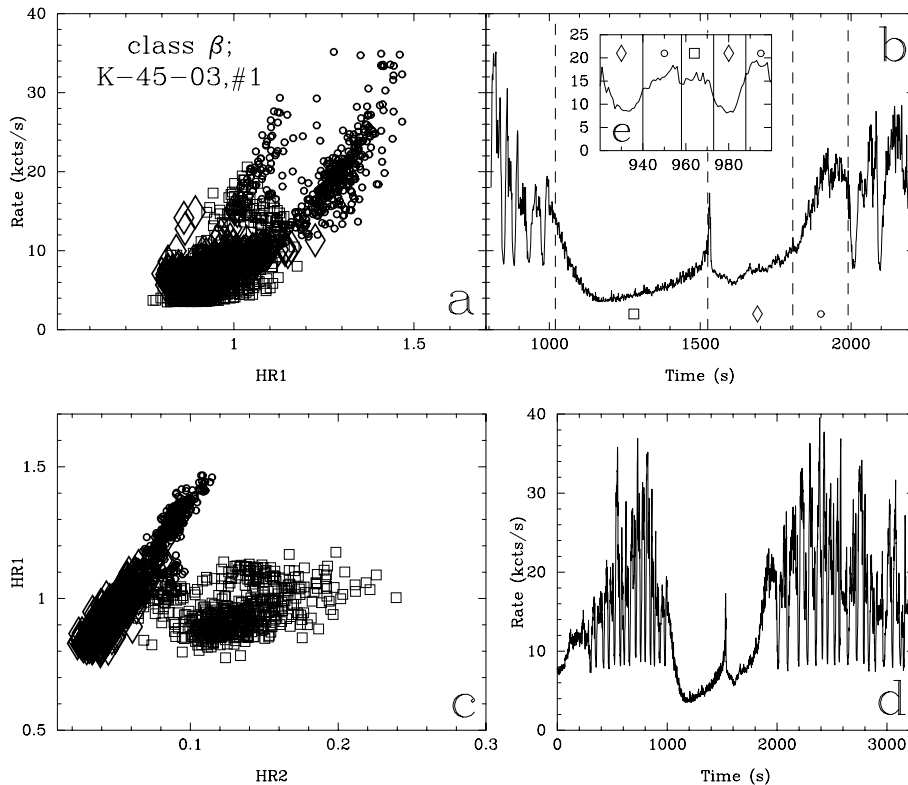
and it shows a great resemblance with the CD's seen in class λ (Fig. 4). In order to identify the different states in the observation shown in Fig. 20, we make use of the similarities with the other classes, as mentioned above. From comparison with class θ (Fig. 6), we can therefore identify state C and A in the quiet interval, as indicated in Fig. 20b. The positions in the CD for these states are the same as found in class θ (see Fig. 6c): a relatively soft state A (below HR1=1.0 and HR2=0.1) and a state C which is much harder in HR2 ($\sim$0.12). As we have seen in the previous sections, after state A the source can make a fast transition into state B, as seen for instance in class λ (Fig. 4b). However, in the case presented here the transition to state B is much more gradual. The spectrum becomes progressively harder, resulting in a connection between state A and B in the CD (the diagonal "finger-like" structure). The quiet interval therefore contains all the three states A,B and C. As mentioned before, the periods showing the large variability are rather similar to the ones shown in class λ (Fig. 5). Only here the large dips all have the same count rate ($\sim$ 8 kcts/s, see Fig. 20b,d), whereas in class λ not only the average count rate in the dips is higher ($\sim$ 12 kcts/s), but also different count rates are observed there (Fig. 5b). Nevertheless we can conclude that during these large variations, as for the ones seen in class λ, the source is switching between all the three states A,B and C. This can be seen by comparing Fig. 5b with Fig. 20e, where a part of the variation interval is shown. The only difference is that in Fig. 20e the state A intervals have a lower count rate than the state C ones. As a result of this oscillating between states during these variations, two branches for state B appear in the HID (Fig. 20a). When the source moves from state A to state B it follows the branch on the right in the

HID, but the transition from state B back to A is characterized by a softer HR1 ($\sim$1), thus following the branch on the left. It is also possible, as explained before, to make the transition from state B to state C. The source then again follows the left branch, but makes a turn to higher HR2 values as it moves to state C. The presence of two branches corresponding to state B will be discussed in the next Section. Notice that class β is the one that has most extensively been studied, especially in multi-wavelength campaigns (see Markwardt et al. 1999; Eikenberry et al. 1998). It is clearly the most complex and possibly the most important of all our 12 classes, and it is presented last here only because in order to understand its structure one needs to examine simple classes first. Its analogies and differences with class λ are very important, but a complete analysis of them is beyond the scope of this paper.

4. Discussion

4.1. The disk-instability model: states B and C

In the previous sections, we classified and described in detail the whole complex phenomenology displayed by GRS 1915+105 in the first two years of RXTE observations. Despite the extreme variety of behavior, our analysis allowed us to identify three main states, the alternation of which are at the base of all the light curves and CDs included in Table 1. While all that has been said before is completely model-independent, we will now discuss the results in terms of the "standard" spectral model consisting of a disk-blackbody component and a power law. The three states can be characterized (and identified) in the following way:

– State A: CD position well above the power-law line (i.e., with a substantial contribution to the flux by a disk component with kT>1 keV). Mostly little time variability, sometimes red-noise variability.
– State B: CD position above the power law line, higher than state A. Substantial red-noise variability on time scales > 1s.
– State C: CD position upon or below power law line (either no disk contribution or very soft disk inner temperature ($\sim$0.5 keV). White noise variability seen on time scales of 1s.

If no structured variability is present in an observation (i.e. classes ϕ and χ), state C can be distinguished from the others by the position in the CD with respect to the power-law line, while state A and state B differ by their value of HR$_1$. State A has HR$_1$ <1.1, state B has HR$_1$ >1.1. In all the other cases, states A and B can only be separated by comparing the points in the CD: state A points are either softer or fainter than state B points.

Notice that a crude subdivision in states, based on a single observation (K-45-03, class β) has been presented by Markwardt et al. (1999). Their "quiet state", "low-frequency noise state" and "1-15 Hz state" can be identified as specific instances of our A,B,C states. respectively. Following Belloni et al. (1997a,b), from the position in the CD, we can identify state B with the typical situation observed in black-hole candidates in high-flux states: the energy spectrum is the superposition of a thermal component originating from an accretion disk which is observable down to the innermost stable orbit, and of a power-law component with a steep slope (see Belloni et al. 1997a; Markwardt et al. 1999). With the same spectral model, in state C the power-law component is much more dominant and the disk component softer. Let us compare our analysis with proposed models, abandoning for the moment our model-independency. In the model by Belloni et al. (1997a,b), this state corresponds to the unobservability of the inner portion of the accretion disk, due to the onset of an instability. As the refill time τ_{refill} is related to the viscous time scale at the inner edge R$_{in}$of the observable part of the disk, the re-fill time for the inner region is

$$\tau_{refill} \propto R_{in}^{3.5}\dot{M}^{-2} \qquad (1)$$

This means that the larger the region affected by the instability, the longer the state-C event will last. From Belloni et al. (1997b), although their definition of CD is slightly different from that used in the present work, we can see that the longer the state-C event, the harder the X-ray colors. Since in state C, as compared to state B, the disk component becomes softer, this means that in state C the power-law component hardens. This effect is observable in our data too: the longer state-C events are located to the right in the CD (see Fig. 2). Therefore, our analysis is in agreement with the disk-instability model, although of course a detailed spectral modeling of all observations would be needed to say something more firm.

4.2. Long-lasting effects of the instability

As we have seen, during the three long quiet intervals included in our sample, the CD analysis shows that the spectrum of GRS 1915+105 is in first approximation consistent with a pure power law, possibly with a high-energy cutoff. All these observations have been identified with state C, and since they appear in three separate long events, it is natural to associate each single long quiet period with a single state C event. In the framework of the disk-instability model applied to GRS 1915+105 it is indeed possible to have a re-filling phase that lasts for a month or more. This can be achieved with a large radius of the unobservable inner region of the disk, which as we have seen is associated with a softening of the disk component and a flattening of the power-law component. During these periods, the soft component becomes therefore so soft that it is not detected anymore (due to the high value of interstellar absorption) and the power-law component becomes progressively harder (see Fig. 11). However, the instability model applies only to the inner radiation-pressure-dominated region of a Shakura & Sunyaev (1973) accretion disk, which for reasonable parameters cannot extend beyond a few hundred kilometers from the black hole. This means that in order to reach the relevant time scales, the accretion rate $\dot{M}$ must also be lower (notice the strong dependence of τ_{refill} on $\dot{M}$). The association between the long quiet periods and single state-C events is strengthened by the observed properties of the 1-10 Hz QPOs in both cases (Markwardt et al. 1999; Muno et al. 1999; Trudolyubov et al. 1999). Muno et al. (1999), in their analysis of a large number of RXTE observations, find a correlation between the frequency of the 1-10 Hz QPO and the inner radius of the accretion disk (as measured through spectral fits). If during the quiet intervals the disk has a large inner radius (so large that the disk component is not seen in the PCA spectra), following this correlation, the QPO frequency should alwasy be rather small, while it can be as high as 10 Hz (Trudolyubov et al. 1999). However, Belloni et al. (1997b) remarked that what can be measured during an instability phase is the inner disk radius at the beginning of the instability. The slow refilling is not observable in the energy spectrum, while the QPO frequency is indeed seen to increase with time as the disk is refilled. Therefore, what must be associated to a large radius is the *slowest* QPO observed in such an interval, which is about 0.6 Hz (Reig et al., in preparation). This would not be inconsistent with the correlation by Muno et al. (1999).

As we have shown in Sect. 3.4, the differences between different long quiet intervals can be interpreted as differences in N$_H$ (between 2 and 6×10^{22}cm^{-2}), but also as differences in high-energy spectral cutoff. A detailed analysis of the energy spectra from these observations will be reported in a second paper. Notice, however, that a cutoff in the broad-band X-ray spectrum of GRS 1915+105 has been observed by Trudolyubov et al. (1999) for the same set of observations, although their value for the cutoff energy (70-120 keV) appears too high to explain these differences. The presence of a high-energy cutoff is also reported by Muno et al. (1999) and Feroci et al. (1999).

4.3. The soft state (state A)

We have seen that, besides state B and state C, a third state appears in most of the light curves we have analyzed. While in most cases this state is well defined, in some observations a gradual transition between state A and state B is observed, although the transition *to* state A is always sharp. We consider it a different state, rather than the softer end of a variable state B because of the sharp transitions. Looking at the CDs, we can see that in the disk+power-law model, the difference between state A and state B could be due to a difference in power law slope, but only if combined with very specific simultaneous changes in the inner temperature of the disk. Also, the changes in power law slope would be very large. A simpler model is to assume that the inner temperature of the disk changes, since the state A to state B line moves parallel to the disk-blackbody line (see Fig. 14). Preliminary spectral fits indicate that indeed there are variations in the temperature of the disk-blackbody component. If the inner radius of the disk does not change, variations in the temperature of the disk are directly associated with variations in the local accretion rate through the inner radius. To test whether such local variations can happen on time scales below a second, since they are connected to the viscous time scale at the inner edge of the disk, we can take the relation measured by Belloni et al. (1997b) between viscous time scale and radius, and extrapolate it down to their minimum observed inner disk radius of ∼20 km. We obtain a time scale of ∼0.5 s, therefore of the right order of magnitude (differences in average accretion rate will influence this number).

The interpretation of the difference between state A and state B in terms of a difference in inner temperature of the accretion disk is also in agreement with the presence of cases where the transition is gradual. In this framework, the disk changes temperature in response to changes in the local accretion rate, changes which can be gradual or sudden. What makes us consider state A a separate state is the presence of the sudden transitions. In particular, the transitions *to* state A are always fast.

The scenario that emerges from this work is the following. The accretion disk can have different temperatures, depending on the accretion rate. The variations in temperature can sometimes be very fast. This is in principle completely independent of the onset of the instability described in Belloni et al. (1997a,b), since A–B transitions are observed even in absence of instability events. Something similar might be observed in other sources, like in the case of GX 339-4 (Miyamoto et al. 1991). However, whenever the disk instability is at work, it triggers such temperature changes, since as we have shown above at the end of an instability event (when the inner portion of the disk is not observable), the disk switches *always* to state A and *never* directly to state B. This is the only link between the two processes (temperature changes and instability) and can provide important clues on both mechanisms.

4.4. Time variability and the three states

The detailed time variability of GRS 1915+105 has been studied by a number of authors (Morgan et al. 1997; Chen et al. 1997; Trudolyubov et al. 1999; Markwardt et al. 1999; Muno et al. 1999, Feroci et al. 1999; Cui 1999). Following these results, it is interesting to compare the presence of the different QPOs observed in the light curves with the three states described here. The so-called "intermediate" QPO, usually between 1 and 15 Hz, is clearly connected to state C (see Markwardt et al. 1999; Muno et al. 1999; Trudolyubov et al. 1999). As one can see from these works, this QPO appears always and only during the state C intervals. Since the frequency of this QPO is proportional to the observed rate (see Markwardt et al. 1999), it is possible that the QPO is a tracer of the keplerian motion at the (large) inner radius of the observable disk, but no precise measurements support this conjecture. If the 67 Hz QPO (Morgan et al. 1997) is indeed associated to either the keplerian motion or relativistic precession at the innermost stable orbit of the accretion disk (Morgan et al. 1997 Zhang et al. 1997), it should not be observed during state C, when the observable inner radius of the disk is much larger than the innermost stable orbit. Although an exhaustive analysis has not been made, Trudolyubov et al. (1999) do not report a detection of such a QPO in the state-C observations they analyzed. As far as the low-frequency QPOs (in the frequency range well below 0.1 Hz) are concerned, it is clear from our analysis that they are simply caused by the state oscillations presented above.

4.5. How many variability classes?

As we said above, it is not within the purposes of this work to provide a complete classification of all the light curves in terms of the absolute minimum number of possible classes. However, it is interesting to note that the three states described in the previous sections and the state transitions between them could in principle give rise to a much larger variety of light curves, while only a limited number has been observed so far. In particular, some of the classes seem to repeat in an almost indistinguishable manner separated by months or even years. It is therefore clear that the structure of the time variability, i.e. the specific alternation of states, is not controlled by a random parameter, but is related to physical quantities.

4.6. Relation to standard black-hole candidates

It is interesting to note that, when in state B, GRS 1915+105 shows energy spectra and power spectra not unlike those of the so-called Very High State of black-hole candidates (see van der Klis 1995). The energy spectrum is a typical disk component down to a few dozen kilometers radius, plus a rather steep power-law component. The power spectrum is also similar to that of a VHS (see Markwardt et al. 1999; Muno et al. 1999; Belloni 2000a). State A is softer and usually (but not always) less variable, and shows sometimes sharp transitions with state B: something similar, although less spectacular, has been observed in the Very High State of GX 339-4 (the so-called "flip-flops", Miyamoto et al. 1991). We can conclude that when it is observed in one of these two states, GRS 1915+105 does not differ much from a standard black-hole candidate. During state C, an insta-

bility occurs, instability which is not yet observed in any X-ray source, and this is what makes this source peculiar. Also, there is evidence that the instability is related to the ejection of superluminal jets from the source (Pooley & Fender 1997; Eikenberry et al. 1998; Mirabel et al. 1998). Despite the fact that the physical conditions are rather different, the power spectra are very similar to those of "canonical" black-hole candidates in their Intermediate state (Belloni 2000a; Trudolyubov et al. 1999). The energy spectra are also similar to the Intermediate State, with a power-law component with a slope of 2.2-2.5 and a soft component (see Belloni et al. 1997b; Markwardt et al. 1999). The association to the Intermediate State becomes stronger when we look at the long quiet periods: here the power law becomes flatter and reaches 1.8 (see Fig. 11 and Trudolyubov et al. 1999) and the characteristic frequencies in the power spectrum become smaller (Trudolyubov et al. 1999). Both the timing and the spectral features approach those of the canonical Low State. Since a similar instability is not observed in standard sources, we can conclude that most likely the Intermediate State is *not* caused by such an instability, but that the instability mimics the conditions that give rise to an Intermediate State. In other words, the source looks like it is in a "canonical" Intermediate State because the instability produces the necessary conditions for such an energy spectrum and such a power spectrum to being produced, i.e. a missing or invisible inner disk.

4.7. The twelve classes as standard modes?

We have shown that it was possible to classify the remarkable variability of GRS 1915+105 in twelve classes. Although more "modes" of variability might be present, it is remarkable that only a handful of classes can be used to represent all observations. Indeed some patterns repeat almost exactly at a distance of months (see Belloni 2000b). Clearly, the presence of three basic states, even with well defined characteristics, is not enough to explain these features. Despite the almost infinite number of ways to alternate the three states, GRS 1915+105 "chooses" only a few. This indicates the presence of a small number of modes of variability, modes which must be connected to basic properties of the accretion disk.

5. Conclusions

We analyzed a large set of RXTE/PCA observations of GRS 1915+105 by means of X-ray color diagrams. We could classify the light curves in 12 separate classes based on the color variability and the light curve. In each of these classes, we could reduce all source variations to the alternation of three basic states. We interpret one of the states as the product of a thermal-viscous instability as proposed by Belloni et al. (1997a,b), and the other two as reflecting different inner temperatures of the accretion disk. This classification provides the necessary background for a detailed analysis based on spectral fitting.

References

Bailyn C.D., Orosz J.A., McClintock J.E., Remillard R.A., 1995, Nat 378, 157

Belloni, T., 2000a, Proc. of 3rd INTEGRAL Meeting, in press

Belloni T., 2000b, In: "The Neutron Star Black Hole Connection", NATO/ASI, in press.

Belloni T., Méndez M., King A.R., van der Klis M, van Paradijs J., 1997a, ApJ 479, L145

Belloni T., Méndez M., King A.R., van der Klis M, van Paradijs J., 1997b, ApJ 488, L109

Castro-Tirado A.J., Brandt S., Lund S., 1992, IAU Circ. 5590

Castro-Tirado A.J., Brandt S., Lund N., et al., 1994, ApJS 92, 469

Cui W., 1999, ApJ 524, L59

Dickey J.M., Lockman F.J., 1990, ARA&A 28, 215

Chen X., Swank J.H., Taam R.E., 1997, ApJ 477, L41

Eikenberry S.S., Matthews K., Morgan E.H., Remillard R.A., Nelson R.W., 1998, ApJ 494, L61

Fender R.P., Pooley G.G., Brocksopp C., Newell S.J., 1997, MNRAS 290, L65

Fender R.P., Pooley G.G., 1998, MNRAS 300, 573

Fender R.P., Garrington S.T., McKay D.J., et al., 1999, MNRAS 304, 865

Feroci M., Matt G., Pooley G., et al., T., 1999, A&A 351, 985

Frank J., King A., Raine D., 1992, *"Accretion power in Astrophysics"*, Cambridge University Press, Cambridge

Greiner J., Morgan E., Remillard R.A., 1996, ApJ 473, L107

Markwardt C.B., Swank J.H., Taam R.E., 1999, ApJ 513, L37

Mirabel I.F., Rodríguez L.F., 1994, Nat 371, 46

Mirabel I.F., Duc P.A., Rodríguez P.A., et al., 1994, A&A 282,L17

Mirabel I.F., Dhawan V., Chaty S., et al., 1998, A&A 330, L9

Mitsuda K., Inoue H., Koyama, K., et al., 1984, PASJ 36, 741

Miyamoto S., Kimura K., Kitamoto S., Dotani T., Ebisawa K., 1991, ApJ 383, 784

Muno M.P., Morgan E.H., Remillard R.A., 1999, ApJ 527, 321

Morgan E., Remillard R.A., Greiner J., 1997, ApJ 482, 993

Nayakshin S., Rappaport S., Melia F., 1999, ApJ, in press

Paciesas W.S., Deal K.J., Harmon B.A., et al., 1996, A&AS, 120, 205

Pooley G.G., 1995, IAU Circ., 6269

Pooley G.G., Fender R.P., 1997, MNRAS 292, 925

Remillard R.A., Morgan E.H., 1998, Nucl. Phys. B (Proc. Suppl.), 69/1-3, 316

Rees M.J., 1966, Nat 211, 468

Rodríguez L.F., Mirabel I.F., 1999, ApJ 511, 398

Sazonov S.Y., Sunyaev R.A., Lapshov, I.Y., et al., 1994, Astr. Lett. 20, 787

Shakura N.I., Sunyaev R.A., 1973, A&A 24, 337

Taam R.E., Chen X., Swank J.H., 1997, ApJ 485, L83

Tanaka,Y., Lewin W.H.G., 1995, In: Lewin W.H.G., Van Paradijs J., Van den Heuvel E.P.J. (eds.) "X-ray binaries", Cambridge Univ. Press., Cambridge, p2.

Trudolyubov S., Churazov E., Gilfanov M., 1999, Astr. Lett. 25, 718

van der Klis M., 1995, In: Lewin W.H.G., Van Paradijs J., Van den Heuvel, E.P.J. (eds.) "X-ray binaries", 1995, Cambridge Univ. Press., Cambridge, p252.

Vilhu O., Nevalainen J., 1998, ApJ 508, L85.

Zhang S.N., Wilson C.A., Harmon B.A., et al., 1994, IAU Circ. 6046

Zhang S.N., Cui W., Chen W., 1997, ApJ 482, L155